actuators

MDPI

Article

Development of Rehabilitation Glove: Soft Robot Approach

Tomislav Bazina [1,2,3], Marko Kladarić [1], Ervin Kamenar [1,2,3] and Goran Gregov [1,*]

[1] University of Rijeka, Faculty of Engineering, Vukovarska 58, 51000 Rijeka, Croatia; tomislav.bazina@uniri.hr (T.B.); markokladar737@gmail.com (M.K.); ekamenar@uniri.hr (E.K.)
[2] University of Rijeka, Center for Micro- and Nanosciences and Technologies, Radmile Matejčić 2, 51000 Rijeka, Croatia
[3] University of Rijeka, Center for Artificial Intelligence and Cybersecurity, Radmile Matejčić 2, 51000 Rijeka, Croatia
* Correspondence: goran.gregov@uniri.hr; Tel.: +385-(0)51-651-528

Abstract: This study describes the design, simulation, and development process of a rehabilitation glove driven by soft pneumatic actuators. A new, innovative finger soft actuator design has been developed through detailed kinematic and workspace analysis of anatomical fingers and their actuators. The actuator design combines cylindrical and ribbed geometries with a reinforcing element—a thicker, less extensible structure—resulting in an asymmetric cylindrical bellow actuator driven by positive pressure. The performance of the newly designed actuator for the rehabilitation glove was validated through numerical simulation in open-source software. The simulation results indicate actuators' compatibility with human finger trajectories. Additionally, a rehabilitation glove was 3D-printed from soft materials, and the actuator's flexibility and airtightness were analyzed across different wall thicknesses. The 0.8 mm wall thickness and thermoplastic polyurethane (TPU) material were chosen for the final design. Experiments confirmed a strong linear relationship between bending angle and pressure variations, as well as joint elongation and pressure changes. Next, pseudo-rigid kinematic models were developed for the index and little finger soft actuators, based solely on pressure and link lengths. The workspace of the soft actuator, derived through forward kinematics, was visually compared to that of the anatomical finger and experimentally recorded data. Finally, an ergonomic assessment of the complete rehabilitation glove in interaction with the human hand was conducted.

Keywords: soft robotics; rehabilitation glove; pneumatic actuators; pseudo-rigid kinematic model

check for updates

Citation: Bazina, T.; Kladarić, M.; Kamenar, E.; Gregov, G. Development of Rehabilitation Glove: Soft Robot Approach. *Actuators* **2024**, *13*, 472. https://doi.org/10.3390/act13120472

Academic Editor: Daniele Leonardis

Received: 15 October 2024
Revised: 12 November 2024
Accepted: 21 November 2024
Published: 22 November 2024

Copyright: © 2024 by the authors. Licensee MDPI, Basel, Switzerland. This article is an open access article distributed under the terms and conditions of the Creative Commons Attribution (CC BY) license (https://creativecommons.org/licenses/by/4.0/).

1. Introduction

The rising global incidence of hand function impairments, often resulting from various neurological disorders and musculoskeletal diseases such as arthritis, cerebral palsy, Parkinson's disease, stroke, and multiple sclerosis, presents significant challenges in performing activities of daily living (ADL) and represents a growing societal burden [1–3]. Moreover, the aging population is increasingly contributing to higher rates of disability, leading to an inverted pyramid in the age distribution of affected individuals [4]. As a result, stroke, hemiplegia, and related conditions have become critical areas of focus in medical care and rehabilitation, requiring long-term treatment and presenting complex social challenges. A vital approach to enhancing recovery in physical rehabilitation involves promoting motor recovery through repetitive movements, capitalizing on the brain's capacity for neuroplasticity—the formation of new neural connections. When traditional methods are employed, where physical therapists typically work with affected individuals one-on-one, the high demand for medical resources exacerbates the already limited healthcare workforce. This makes it challenging to provide the consistent, frequent, and intensive physical therapy essential for successful recovery [2,5].

Robotic-assisted rehabilitation offers a promising solution, providing effective therapy with minimal dependence on healthcare professionals. Given the intricate anatomy of

the human hand, which features up to 25 degrees of freedom (DOFs) and is designed for performing both precise and powerful gripping tasks, the need for advanced rehabilitation methods is evident [1,6]. In response to these challenges, rehabilitation robots built on soft robotic principles present a viable solution, offering a more adaptive approach to therapy compared to traditional rigid robots due to their inherent safety, flexibility, and more versatile designs [3,7–9]. Authors in [10] proved the effectiveness of using a soft robotic rehabilitation glove for patients with spinal cord injuries.

One similar approach is demonstrated in [11], where the authors developed a robotic glove using soft actuators from composite tubular constructions with anisotropic fiber reinforcements embedded in an elastomeric matrix. These actuators, fabricated in four stages, are designed to mimic finger movements through fluid pressurization, generating significant force when pressurized and exhibiting low impedance when inactive. The actuators effectively replicate finger and thumb motions for typical grasping tasks. A related example is presented in [12], where the authors investigated a 3D-printed soft robotic hand exoskeleton featuring a novel fold-based actuator design. They provided fabrication guidelines, characterized its range of motion (ROM) and grip force, and proposed future revisions to more closely match the ROM of a healthy hand. Similar studies that introduce the design and validation of 3D-printed soft actuators for developing glove rehabilitation devices are presented in [13,14]. Another study [15] presents a soft robotic glove system with a high power-to-weight ratio and enhanced ergonomics. The glove utilizes a bidirectional linear soft actuator and soft orifice valves with cable transmission for synchronized finger actuation. Although various concepts have been proposed, as also comprehensively reviewed by the authors in [3]—covering devices primarily based on cable-driven, pneumatic, and hydraulic actuators—the need for further advancements in actuator design, safety, and implementation remains essential.

This work aims to develop a rehabilitation glove prototype utilizing a soft robotics approach with positive pressure actuation. Our contribution advances the field by introducing a method for developing functional, fully 3D-printed soft actuators designed to drive the rehabilitation glove. The design process for the finger actuators begins with a comprehensive kinematic analysis based on a simplified model of human hand kinematics and its reachable workspace, building upon our previous research [1,16]. The reachable workspace then serves as the foundation for the kinematic characterization of the soft actuator, allowing us to derive a 3D model of the glove that covers the fingers' functional ROM. We also introduce pseudo-rigid kinematic models for the finger-soft robots, relying solely on pressure and link lengths. This approach effectively applies conventional rigid robotics methods to model soft robotic devices. Figure 1 provides a graphical summary of the proposed development approach.

The remainder of the paper is organized as follows: Section 2 presents the approximation of the soft robot kinematics using a pseudo-rigid model [17] and modified Denavit–Hartenberg (DH) [18] approach. We then propose a design for a soft rehabilitation glove, which we numerically evaluate and manufacture using 3D printing techniques. In Section 3, we conduct an experimental assessment of the soft robotic glove, introduce finger-specific constraints, and present the obtained workspace trajectories.

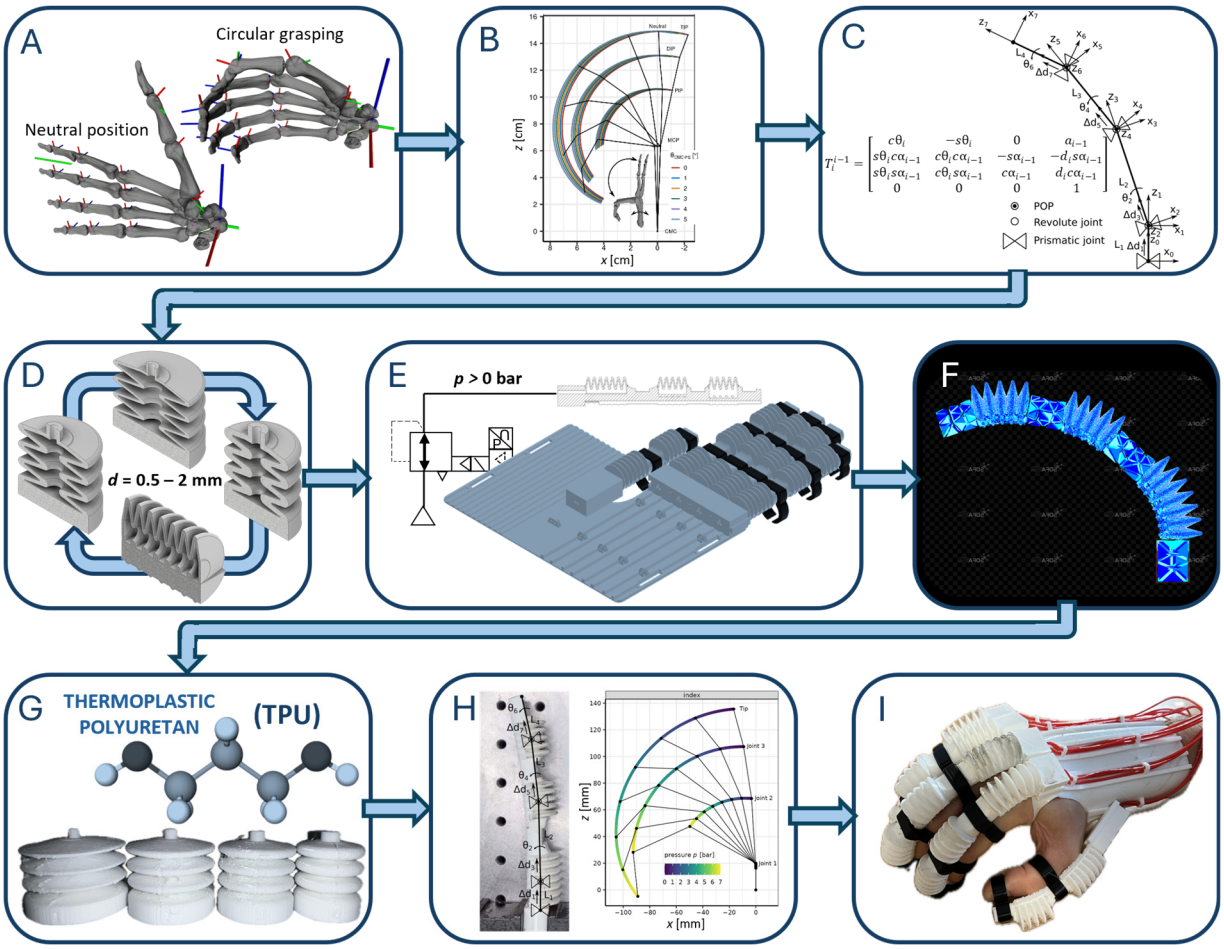


Figure 1. The process of design, development, and experimental assessment of the rehabilitation glove: (**A**) circular grasping example; (**B**) finger ROM; (**C**) finger kinematics; (**D**) tuning of construction parameters in the design process; (**E**) final 3D model; (**F**) SOFA simulation; (**G**) 3D-printed segments made from TPU, featuring varying dimensions and wall thicknesses for design analysis; (**H**) experimental assessment and validation of the soft robot's ROM; and (**I**) the developed rehabilitation glove fitted onto the user's hand.

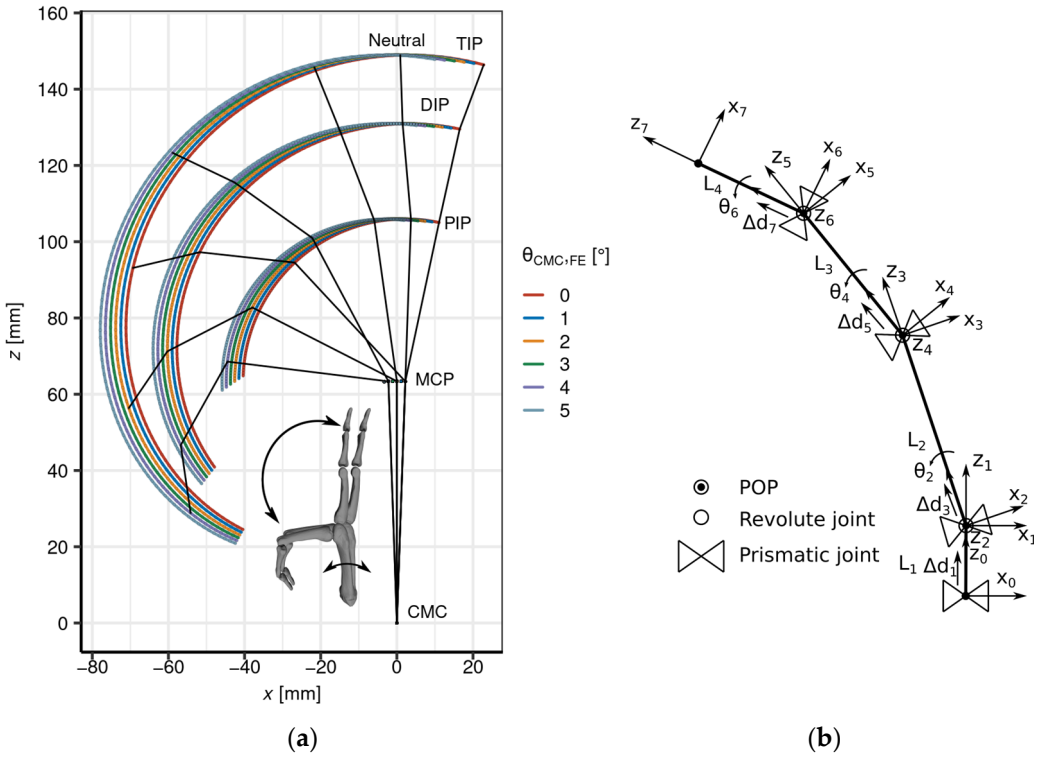
2. Materials and Methods

The core concept of the design is based on the operating principle of bending pneumatic soft actuators driven by positive pressure. The actuator achieves bending in one direction through a flexible segment, while a more rigid segment limits movement in the opposite direction, causing the actuator to bend when positive pressure is applied. Based on the aforementioned operating principle, two flexible segment morphologies are identified: ribbed cylindrical and pleated segment morphologies [19]. We have prioritized 3D printing with flexible filament for the rehabilitation glove prototype, enabling rapid and cost-effective prototyping.

Before designing the soft glove actuators, we first analyze the kinematics of the human finger to ensure compatibility during circular grasping. We adopt the approach of reducing complexity from 24 to 9 DOFs while enhancing accuracy by incorporating finger curvatures [16]. Compatibility and smooth interaction are achieved through functional tracking of adjacent finger trajectories, covering the full ROM. Additionally, based on the analysis of intra-finger dependencies during flexion and extension using data from 23 daily movements across 77 subjects, as well as agglomerative clustering of the models in [1], we effectively balanced model accuracy and complexity, reducing the required DOFs.

2.1. Kinematic Characterization of a Soft Robot Using a Pseudo-Rigid Approach

As a basis for the kinematic modeling of soft robot actuators, we use results from our previous work [16], which presents a detailed kinematic analysis of the anthropometric hand model encompassing inter- and intra-joint constraints and implementation in an open-source environment. Four fingers—the index (I), middle (M), ring (R), and little (L)—were represented using a single kinematic tree with different parameters and constraints (see [16]). Joint parameters were obtained using a modified DH approach, and a reachability analysis of the fingers' workspace was performed. Kinematic trajectories for I finger anatomical joints—carpometacarpal (CMC), metacarpophalangeal (MCP), proximal interphalangeal (PIP), distal interphalangeal (DIP), and fingertip (TIP)—in the flexion-extension (FE) plane are depicted in Figure 2a.



(**a**) (**b**)

Figure 2. Kinematic analysis: (**a**) workspace of the index finger in FE plane with finger joint (MCP, PIP, DIP, TIP) trajectories during circular grasping according to [16] and (**b**) soft finger actuator kinematic chain with modified DH approach. The diagram displays revolute and prismatic joints along the robot's segments, with symbols indicating points of rotation (POP), revolute joints, and prismatic joints. Each joint is labeled with corresponding DH parameters, including joint angle (θ_i) and elongation (Δd_i).

Based on the above-described analysis of human finger reachability, we devised a pseudo-rigid model [17] to represent the kinematics of the compatible soft robotic finger actuator. In the pseudo-rigid approach, soft robots are described using rigid links connected by joints. Each joint constitutes one DOF to enable relative motion. Our analysis used revolute joints, representing rotations, and prismatic joints, representing linear offset. Three revolute joints enable motion corresponding to the finger MCP, PIP, and DIP anatomical joints. At the same time, we introduced four additional prismatic joints to compensate for misalignments between finger and actuator trajectories. One soft robot actuator thus comprises 7 DOFs. Following a modified Denavit–Hartenberg (DH) convention [18], we assigned eight frames (0–7) to links from the base to the tip of the actuator. Frames are rigidly attached to links, and transformations between frames describe relative link translations and rotations. The kinematic chain of the soft robot actuator is schematically represented in Figure 2b, with the y_i-axes omitted for brevity. For revolute joints, the joint

axis is defined as the axis of revolution, while for prismatic joints, it is the axis of translation. Likewise, revolute joint parameters are denoted by joint angles θ_i, while prismatic with link offsets d_i. The entire procedure of assigning frames to links for axis pairs $(i, i+1)$ is the following [18]:

1. Place the origin of the i-th frame at the intersection of two axes or where the common perpendicular meets the i-th axis.
2. Align the z_i axis along the i-th joint axis.
3. Point the x_i axis along the common perpendicular, or if the axes intersect, make x_i perpendicular to the plane containing both axes.
4. Align frame 0 with frame 1 when the first joint parameter is zero.
5. For the origin n-th frame, pick x_n arbitrary to simplify joint parameters.

Now, the four DH parameters (Table 1) of the soft robot actuator can be obtained as follows:

- α_{i-1}: angle from z_{i-1} to z_i around x_{i-1},
- a_{i-1}: distance from z_{i-1} to z_i along x_{i-1},
- d_i: distance from x_{i-1} to x_i along z_i,
- θ_i: angle from x_{i-1} to x_i around z_i.

Table 1. Modified DH parameters for soft robot actuator.

Link i	α_{i-1}	a_{i-1}	d_i	θ_i
1	0	0	$L_1 + \Delta d_1$	0
2	$\pi/2$	0	0	θ_2
3	$-\pi/2$	0	$L_2 + \Delta d_3$	0
4	$\pi/2$	0	0	θ_4
5	$-\pi/2$	0	$L_3 + \Delta d_5$	0
6	$\pi/2$	0	0	θ_6
7	$-\pi/2$	0	$L_4 + \Delta d_7$	0

As a last forward kinematics step, homogeneous transformation matrices can be used to describe the position and orientation of the actuator joints relative to the base frame 0. To fully define 3D position and 3D orientation, 6D transformation has to be employed. The general form of the transformation matrix between $(i-1)$-th and i-th frame, consisting of a 3×3 rotational matrix R_i^{i-1} and a 3×1 translation vector P_i^{i-1}, is derived through two screw-like transformations; first, a translation along a_{i-1} followed by a rotation about α_{i-1}, and then a translation along d_i followed by a rotation about θ_i [18]

$$T_i^{i-1} = \begin{bmatrix} & R_i^{i-1} & & P_i^{i-1} \\ 0 & 0 & 0 & 1 \end{bmatrix} = \begin{bmatrix} c\theta_i & -s\theta_i & 0 & a_{i-1} \\ s\theta_i c\alpha_{i-1} & c\theta_i c\alpha_{i-1} & -s\alpha_{i-1} & -d_i s\alpha_{i-1} \\ s\theta_i s\alpha_{i-1} & c\theta_i s\alpha_{i-1} & c\alpha_{i-1} & d_i c\alpha_{i-1} \\ 0 & 0 & 0 & 1 \end{bmatrix}, \quad (1)$$

where simplifying notation symbols are defined as follows:

$$\begin{aligned} c\theta_i \Longrightarrow \cos\theta_i; \quad s\theta_i \Longrightarrow \sin\theta_i \quad \forall i \in [1,7], \\ c\alpha_{i-1} \Longrightarrow \cos\alpha_{i-1}; \quad s\alpha_{i-1} \Longrightarrow \sin\alpha_{i-1} \quad \forall i \in [1,7]. \end{aligned} \quad (2)$$

Using DH parameters from Table 1, transformation matrices between each pair of neighboring frames $T_1^0, T_2^1, T_3^2, T_4^3, T_5^4, T_6^5, T_7^6$ were obtained. The transformation matrix for the tip of the soft actuator, defining its position and orientation relative to the base frame 0, is obtained by multiplying all transformation matrices along the kinematic chain

$$T_7^0 = T_1^0 T_2^1 T_3^2 T_4^3 T_5^4 T_6^5 T_7^6 = \begin{bmatrix} c\theta_{246} & 0 & -s\theta_{246} & -d_3 s\theta_2 - d_5 s\theta_{24} - d_7 s\theta_{246} \\ 0 & 1 & 0 & 0 \\ s\theta_{246} & 0 & c\theta_{246} & c\theta_2 d_3 + c\theta_{24} d_5 + c\theta_{246} d_7 + d_1 \\ 0 & 0 & 0 & 1 \end{bmatrix}, \quad (3)$$

where simplifying notation symbols are defined as follows:

$$\begin{aligned} c\theta_{24} &= \cos(\theta_2 + \theta_4), \quad & c\theta_{246} &= \cos(\theta_2 + \theta_4 + \theta_6), \\ s\theta_{24} &= \sin(\theta_2 + \theta_4), \quad & s\theta_{246} &= \sin(\theta_2 + \theta_4 + \theta_6). \end{aligned} \quad (4)$$

2.2. Design and Development of a Soft-Robotics-Based Rehabilitation Glove

After conducting an in-depth kinematic analysis of a soft robot finger, based on the reachable workspace of the human hand, we present a conceptual design for a rehabilitative glove that utilizes pneumatic principles and 3D printing technology. In examining existing design solutions for soft pneumatic actuators with bending capabilities, we observed that most feature an external cylindrical geometry. This design simplifies manufacturing compared to other shapes and enables the actuator to achieve significant blocking forces. Moreover, the cylindrical form enhances ergonomic performance, particularly in applications involving close interaction with the human body. Furthermore, the ribbed geometry in soft pneumatic actuators is designed as a bellow, leading to the development of bellow pneumatic actuators, also known as bellow pneumatic muscle actuators (PMA) [20]. The main advantages of bellow PMAs are their high contraction ratio, significant maximum force relative to their dimension, and cost-effectiveness. Additionally, the ribbed geometry facilitates significant bending angles, making it well-suited for actuators that operate effectively during angular movement. Two primary design principles achieve angular movement in soft pneumatic actuators. The first principle involves incorporating a limiting element with plated geometry, typically positioned inside the actuator. When pressure or vacuum is applied, this element restricts contraction on one side, causing the actuator to bend on the opposite side. The second principle entails designing the actuator with an asymmetrical shape, resulting in bending as the geometry on one side contracts more than the other.

Building on the advantages of various geometric shapes in soft pneumatic actuators, as highlighted by Marchese et al. [19], we developed a hybrid design solution for the rehabilitative glove's actuator. This design combines cylindrical and ribbed geometries with a constraining element in the form of a thicker, less extensible structure. The result is a cylindrical bellow actuator with an asymmetrical shape, featuring a reinforced layer on one side. A cross-section of one segment is shown in Figure 3a. As previously mentioned, the I, L, R, and M fingers require the actuation of three joints (see Figure 3b), leading to a design that incorporates three actuator segments and cylindrical components corresponding to the finger's phalanges. Figure 3c illustrates the cross-section of the model, showing all three sections along with channels for the delivery of pressurized air to each segment. To ensure the supply of compressed air to each actuator segment, cylindrical channels connect the actuators to the pneumatic supply pipes, with the connection achieved using a sealant. To ensure ergonomic and soft contact between the glove actuator and the human fingers, a rounded groove is designed on the side of the actuator featuring flat geometry. Grooves are incorporated into the cylindrical segments to accommodate ring-shaped elements, facilitating the transfer of force and movement from the actuators to the fingers. A supporting element that secures all the actuators in position and attaches the device to the human hand is depicted in Figure 3d. The glove's supporting element is designed to be flexible, allowing it to adapt to the human hand. It features triangular protrusions that facilitate positioning and create a secure fit with the finger actuators. Additionally, the support element features holders that guide the pneumatic tubes, ensuring they are correctly positioned and integrated as part of the glove. On the interlocking side of the

actuator, a prismatic segment with triangular protrusions and grooves has been designed to connect the actuators to one another and to the support element. The dimensions of each soft actuator are given in Table 2.

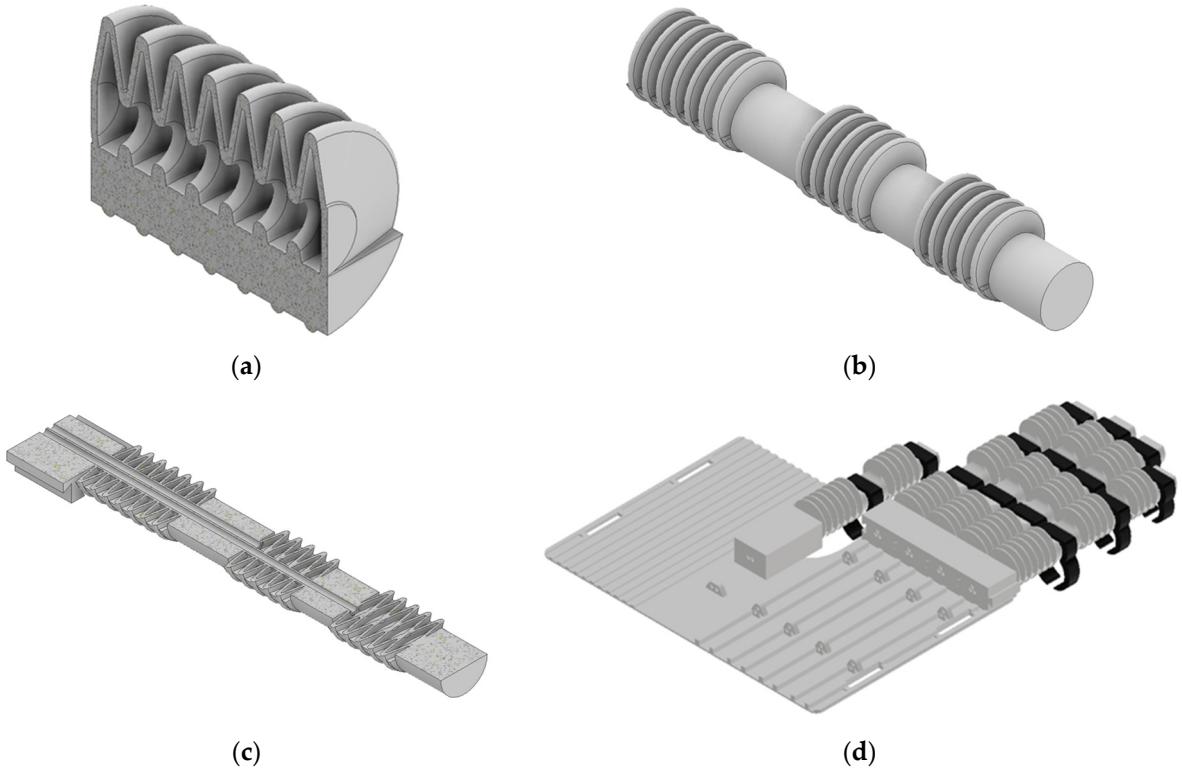
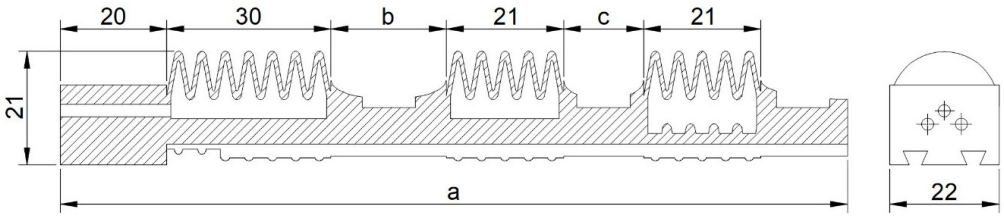


Figure 3. A 3D model of the rehabilitation glove: (**a**) cross-sectional view of a single actuating element; (**b**) finger actuator composed of three segments; (**c**) cross-sectional view of cylindrical channels for compressed air supply; and (**d**) assembly of the 3D model of the rehabilitation glove.

Table 2. Dimensions of soft actuators for the rehabilitation glove.



Finger	*a* [mm]	*b* [mm]	*c* [mm]
Thumb	125	19	-
Index	147	22	15
Middle	151	24	17
Ring	149	22	17
Little	135	19	13

During the conceptual phase of the rehabilitative glove, we opted for 3D printing with flexible filament for the fabrication process. Unlike methods such as [11], where actuators are manufactured in several phases, our design and 3D printing approach enable the construction of each actuator in a single step. The entire glove, including both the soft pneumatic actuators and the supporting element, is fabricated using flexible material to allow for bending. The supporting element wraps around the hand and is secured with hook-and-loop fasteners. Designing this element was challenging, as it required precise

positioning of both the support structure and the pneumatic actuators relative to the user's hand and fingers, necessitating several design iterations during development.

2.3. Numerical Validation of the Rehabilitation Glove

Based on the proposed rehabilitation glove model, we conducted a preliminary simulation analysis of its soft pneumatic actuators under varying pressure values to ensure proper functionality and determine the maximum achievable bending angles. This analysis was conducted using the Simulation Open Framework Architecture (SOFA (https://www.sofa-framework.org/, accessed on 21 November 2024)) software, an open-source platform widely used for medical simulations [21]. SOFA offers a modular and flexible simulation framework, enabling independently developed algorithms to interact within the same environment, reducing integration time. It uses a scene graph, a hierarchical tree structure of nodes and components, which define and describe the simulation.

The algorithm for simulating the soft actuator is written in Python, using the SofaPython3 (https://sofapython3.readthedocs.io/en/latest/, accessed on 21 November 2024) extension alongside the standard software package to develop simulations. The actuator simulation process begins with discretizing the soft actuator into a volumetric mesh of tetrahedrons, accomplished using the Gmsh (https://gmsh.info/, accessed on 21 November 2024) tool. This tool generates a .vtk file that contains information on node positions and their connectivity. The volumetric mesh of the actuator model is shown in Figure 4a. The mesh is then imported into the Mesh component, and a MechanicalObject component is created to define the DOFs for the actuator's movement.

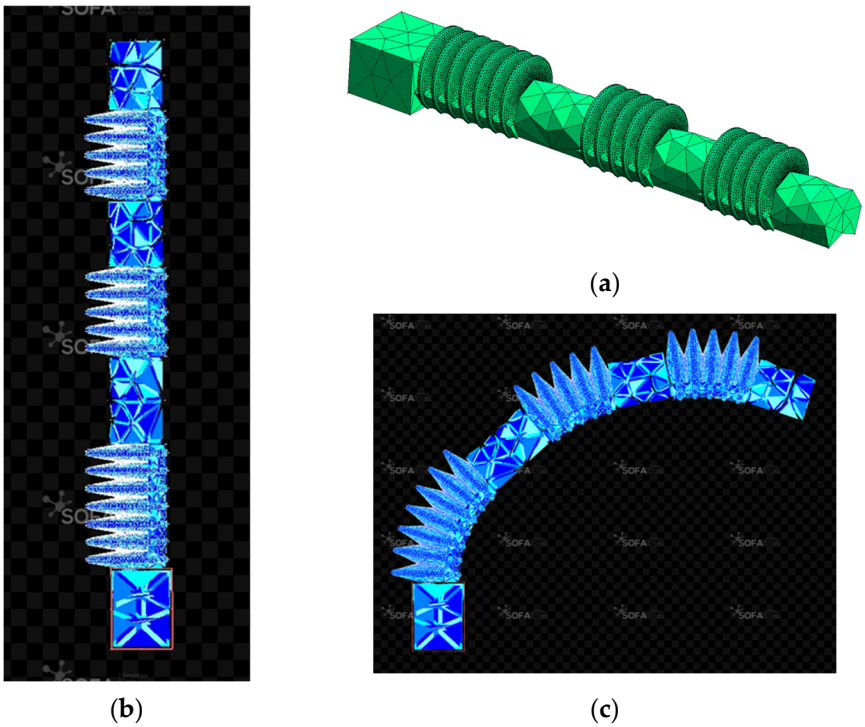


Figure 4. Soft actuator simulation: (**a**) volumetric mesh, (**b**) index finger simulation at 0 bar pressure (initial position), and (**c**) index finger simulation at 8 bar pressure.

Next, the material properties of the actuator are defined by adding a ForceField component, which describes the internal forces generated during the object's deformation, thereby determining the material's elasticity. Within this component, properties such as the elastic modulus (12 MPa) and Poisson's ratio (0.35) are specified. The mass of the actuator (0.05 kg) and the direction of gravitational force also need to be set. To fix the actuator in space, boundary conditions had to be defined for specific object parts. This is achieved using the RestShapeSpringsForceField component, which creates springs between the current

position of a section of the object and its initial position. The stiffness of these springs is adjustable, and by assigning a very high stiffness value, the actuator can be effectively fixed in space chambers within the actuator that will be supplied with air. This is achieved by specifying the DOFs for these chambers using the MechanicalObject component, which allows them to expand as pressure increases during the simulation. Activation can be controlled by varying either the pressure or the volume. For real-time expansion of the cavities, a PythonScriptController is used. This component links to a Python script that performs specific actions during initialization or throughout the simulation and is integrated into the main simulation node. A new class, FingerController, was created to enable incremental pressure increases within the actuator, with each increment set to 1 bar. Finally, the time integration scheme has to be defined, which outlines the system to be solved at each time step of the simulation, as well as the matrix solver used to resolve this system and compute the updated velocities and node positions of the actuators. In this case, the implicit Euler scheme and a direct solver based on LDL decomposition of the matrix were used.

2.4. Fabrication of Rehabilitation Glove

The rehabilitation glove was fabricated using a Prusa i3 MK3S 3D printer. Given the need for flexible characteristics, thermoplastic polyurethane (TPU) was selected as the material. TPU is a versatile polymer commonly utilized in 3D printing for its unique properties, including elasticity, shock absorption, and resistance to oil, grease, and abrasion. A significant advantage of TPU is its ability to create components that can bend and stretch without breaking. Its stretchability ranges from 300% to 600%, allowing it to extend three to six times its original length before failure, making it ideal for applications that require durability and flexibility. The Shore hardness (A scale) of TPU typically ranges from approximately 60 A (silicone-like) to 95 A (firm nylon-like). Additionally, TPU's tensile strength generally varies between 25 MPa and 50 MPa, depending on its specific composition and structure [22].

For printing the rehabilitative glove, TPU with 85 A hardness was selected. The print settings include a bed temperature of 50 °C to enhance the adhesion of the first layer, which is set at 0.25 mm for better foundation, while subsequent layers are 0.2 mm. The printing speed is reduced to 10 mm/s for improved control and precision with the flexible TPU, while the speed between extrusion moves is set to 30 mm/s to minimize transition time and reduce stringing. Filament retraction is disabled (set to 0 mm) to prevent air bubbles and extrusion issues. The infill density is 35% to balance material usage and structural integrity. The cooling fan is turned off to maintain layer adhesion, and the extrusion rate is increased to 105%, with the first layer at 110%, ensuring full material coverage to eliminate gaps and weak spots.

Besides numerical simulation analysis conducted using SOFA v24.06.00 software (see Section 2.3), which considered various wall thicknesses, a performance test was carried out prior to manufacturing the glove prototype due to the specific 3D printing process with TPU material. This test involved fabricating a single soft pneumatic actuator segment with varying wall thicknesses (see Figure 1G). An air pressure of 8 bar was applied to determine the optimal wall thickness that provided the necessary strength and airtightness. Given that the 3D printer nozzle used for extrusion had a diameter of 0.4 mm, the wall thicknesses were set as multiples of this dimension, resulting in options of 0.4 mm, 0.8 mm, 1.2 mm, and 1.6 mm. Based on the test results, the optimal wall thickness for the soft actuator segments was determined to be 0.8 mm. The actuator with a wall thickness of 0.4 mm achieved a greater bending angle; however, after a certain number of activations, the layers of the 3D-printed material started to delaminate. The 0.8 mm wall thickness achieved a slightly reduced bending angle without delamination of the layers, whereas the 1.2 mm thickness produced a considerably smaller bending angle.

Following the 3D printing of each finger actuator, additional rings are made from standard PLA material to connect the actuator to the human finger, ensuring secure attachment. The glove's support structure is also 3D-printed using TPU material, which

provides a comfortable fit around the user's hand. Hook-and-loop straps fasten and adjust the glove, allowing easy customization to fit the user's needs. Once all components are assembled, the glove is connected to the pneumatic tubes. FESTO tubes with catalog number PUN-H 2 × 0.4 and an inner diameter of 1.2 mm were chosen for this purpose. Their smaller diameter is well-suited to the dimensions of the actuators and simplifies attachment to the glove's support structure. The 1.2 mm inner diameter provides adequate airflow for the pneumatic actuators, which operate without requiring high-speed movements. Figure 5a shows the fully assembled soft robotic device mounted on a human hand in the initial position, while Figure 5b illustrates its activated state.



(**a**) (**b**)

Figure 5. Soft-robotic glove fitted to the user's hand: (**a**) all soft actuators in initial position and (**b**) all soft actuators activated.

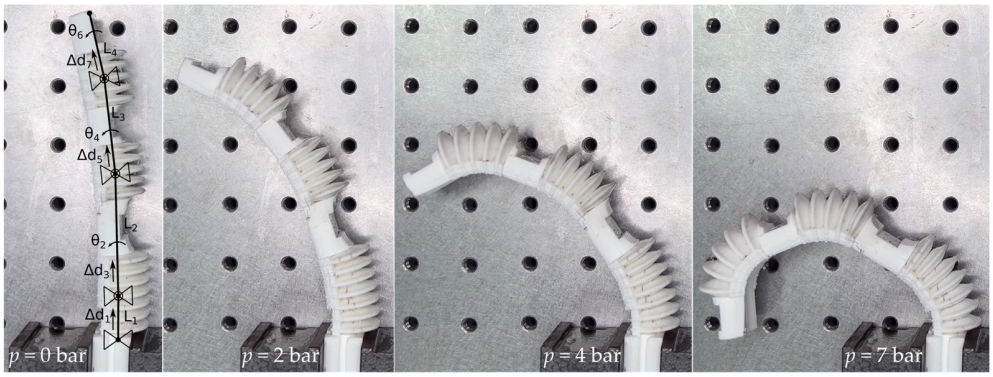
3. Experimental Validation and Results

The experiments were conducted at the Laboratory of Hydraulics and Pneumatics, Faculty of Engineering, University of Rijeka, using the following equipment: a CECCATO CSM 7.5 compressor with an air preparation unit, FESTO distribution manifolds FR-12-M5 with push-in fittings QSM-M5-2, and a FESTO LR-MICRO-MA40-Q4 manual pressure regulator.

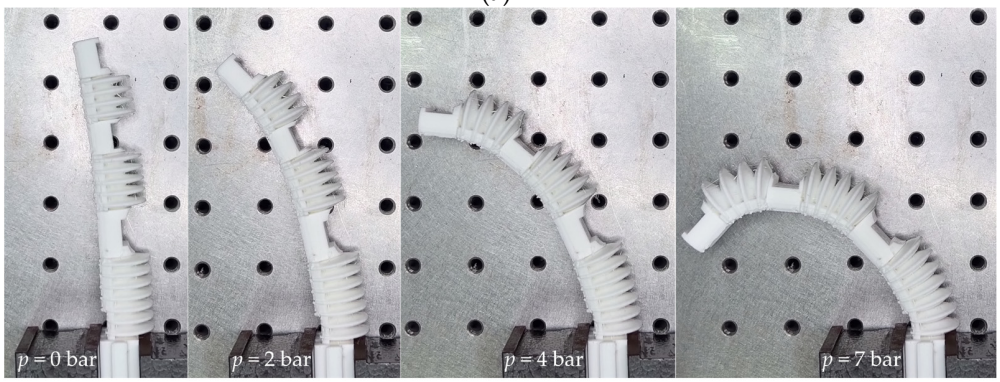
Initially, laboratory tests were performed to evaluate the functionality of the manufactured soft pneumatic actuators, with each finger actuator tested separately. Airtightness was validated by submerging each actuator in a water container while applying a pressure of 8 bar. Air leakages, which occurred primarily at the connection between the actuators and the pipes in several instances, were resolved by applying a two-component sealant. Following these tests, the actuator's angular movement was assessed at various pressure levels. As an example, we present a detailed analysis for the I and L fingers; however, the same approach can be applied to the R and M fingers. Using the pressure regulator mentioned above, the pressure was increased from 0 to 7 bar in 1 bar increments. Please note that the minimum recorded pressure that overcame the material's stiffness and initiated the bending of the actuator was 0.2 bar. The experiment was conducted on all five actuators, each individually secured to the test bench. A high-resolution camera captured images for subsequent analysis of the actuators' dynamic performance.

Figure 6 provides examples of bending for the little and index finger actuators at 0, 2, 4, and 7 bar. Figure 6a additionally shows the overlaid schematic with kinematic parameters on the physical actuator's initial position (p = 0 bar).

We repeated the experiment twice at different pressure levels, measuring link lengths L_i and joint angles θ_i. A slight inclination in the non-actuated state is visible for both actuators, similar to anatomical fingers [16]. Link lengths before elongation are $L_i \in \{16.3, 52.3, 39.3, 29.2\}$ mm for the index finger and $L_i \in \{16.4, 48.3, 34.5, 23.6\}$ mm for the little finger actuators. Link elongations Δd_i were calculated by subtracting the non-actuated link length from the current length for each actuator, segment, and pressure level.



(**a**)



(**b**)

Figure 6. Laboratory experiments demonstrating angular motion of soft actuators under varying pressure levels (0, 2, 4, and 7 bar): (**a**) soft actuators for the index finger with overlaid kinematic representation for p = 0 bar and (**b**) soft actuators for the little finger.

Next, a regression study was performed on the measured joint angles θ_i and link elongations Δd_i to assess their correlation with pressure in all three actuator cylindrical segments across both fingers. The experimentally obtained data and the corresponding linear regression analysis for the index and little fingers, which represent changes in joint angle and link elongation as a function of pressure across all three cylindrical actuator segments, are shown in Figures 7a and 7b, respectively.

Each subplot in Figure 7a shows a clear linear trend, indicating that joint angles for both the I and L fingers increase proportionally with pressure. All joint angles positively correlate with pressure, fitting a strong linear model. Similarly, each subplot in Figure 7b demonstrates that joint elongation across all segments also increases linearly with pressure.

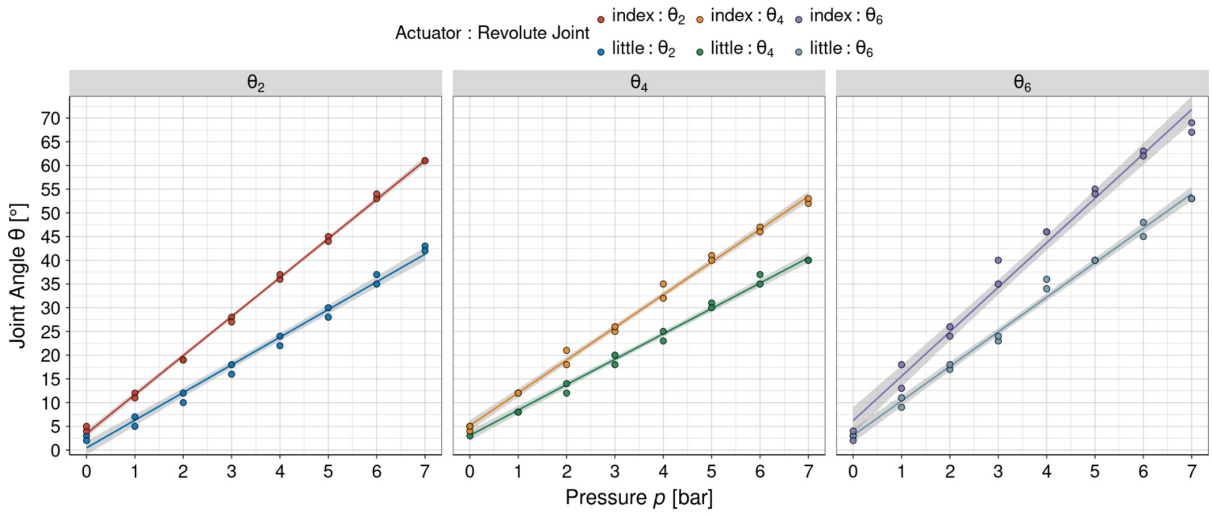
A strong linear trend between joint angle and pressure confirms that the proposed actuator design and material selection provide a consistent stiffness parameter. Additionally, the I-finger actuator achieves a greater bending angle than the L-finger across all three segments. Joint elongations of the I finger also surpass those of the L finger, except in the final segment (from the middle of the last soft joint to the tip), where they are approximately equal.

From the experiment, it can be observed that both the I and L finger soft joints follow a single trajectory during actuation. Thus, additional constraints must be incorporated into the homogeneous transformation to account for joint elongation and angular movement.

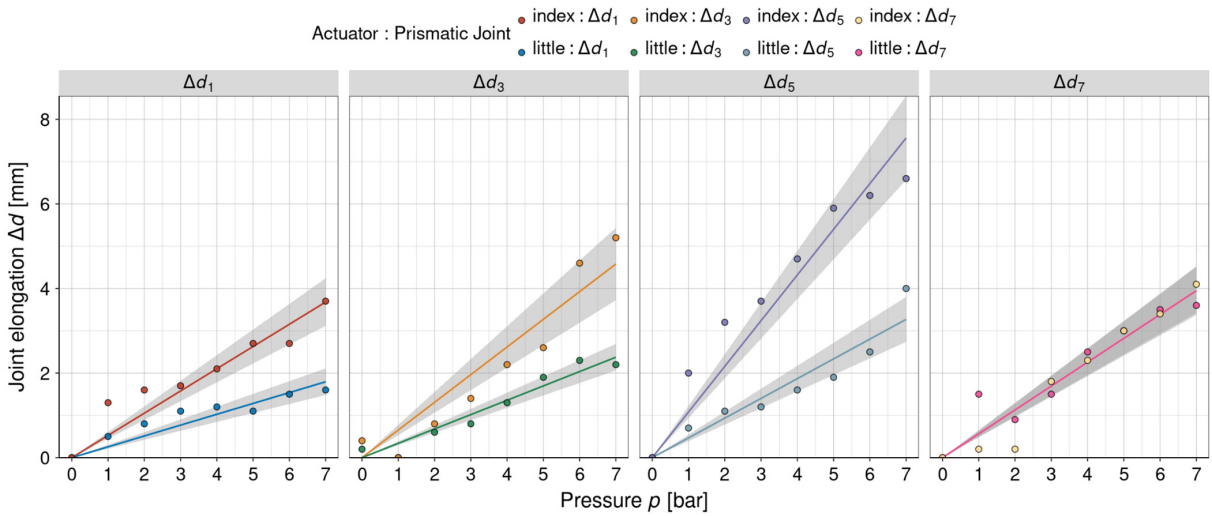
$$\begin{aligned} \theta_i[^\circ] &= \theta_{0,i}[^\circ] + K_{p,i}[^\circ/\text{bar}]p[\text{bar}] \quad \forall i \in \{2,4,6\} \\ \Delta d_i[\text{mm}] &= K_{p,i}[\text{mm/bar}]p[\text{bar}] \quad \forall i \in \{1,3,5,7\} \end{aligned} \tag{5}$$

The linear joint constraints for the I and L fingers, along with their goodness-of-fit indicators, are presented in Table 3. The coefficients of the determination indicate a strong positive relationship between pressure and joint angle (with a minimum R^2 = 0.983), as

well as between pressure and joint elongation (with a minimum $R^2 = 0.952$), following the guidelines for interpreting correlation coefficients [23].



(**a**)



(**b**)

Figure 7. Experimentally obtained linear joint constraints for index and little finger depending on pressure (95% confidence intervals colored in gray): (**a**) revolute joint angle and (**b**) link offset vs. pressure.

Table 3. Linear joint constraints for index and little finger with goodness of fit indicators (R^2—coefficient of determination; SE—standard error).

Finger	Coeff/Joint	θ_2	θ_4	θ_6	Δd_1	Δd_3	Δd_5	Δd_7
Index	Intercept, $\theta_{0,}$, i [°]	3.46	5.17	6.21	–	–	–	–
	Pressure coefficient, $K_{p,i}$ [°/bar] or [mm/bar]	8.23	6.90	9.37	0.53	0.65	1.10	0.57
	Adjusted R^2	0.998	0.995	0.983	0.968	0.952	0.976	0.974
	Residual SE [°] or [mm]	0.788	1.121	2.885	0.401	0.613	0.711	0.39
Little	Intercept, $\theta_{0,}$, i [°]	0.46	3.08	3.08	–	–	–	–
	Pressure coefficient, $K_{p,i}$ [°/bar] or [mm/bar]	5.83	5.35	7.28	0.26	0.34	0.47	0.56
	Adjusted R^2	0.988	0.992	0.992	0.958	0.975	0.964	0.97
	Residual SE [°] or [mm]	1.498	1.104	1.52	0.225	0.225	0.38	0.413

Moreover, the small residual errors—ranging from 0.788 to 2.885 degrees for joint angles and 0.225 to 0.711 mm for elongation—suggest that the linear model accurately captures the soft actuators' inherent compliant behavior.

By inserting the linear constraints defined by Equation (5) into the tip transformation matrix (3) and applying the coefficients from Table 3, we can finally determine the orientation and position of the actuator tip only as a function of the pressure p and the initial link lengths L_i prior to elongation. For the index finger, we obtain

$$T_7^0 = \begin{bmatrix} c_{p,\mathrm{I}} & 0 & -s_{p,\mathrm{I}} & -s_{p,\mathrm{I}}(L_4+0.57p) - (L_2+0.65p)\sin(8.23p+3.46) - (L_3+1.1p)\sin(15.13p+8.63) \\ 0 & 1 & 0 & 0 \\ s_{p,\mathrm{I}} & 0 & c_{p,\mathrm{I}} & L_1 + c_{p,\mathrm{I}}(L_4+0.57p) + 0.53p + (L_2+0.65p)\cos(8.23p+3.46) + (L_3+1.1p)\cos(15.13p+8.63) \\ 0 & 0 & 0 & 1 \end{bmatrix} \tag{6}$$

while for the little finger, we have

$$T_7^0 = \begin{bmatrix} c_{p,\mathrm{L}} & 0 & -s_{p,\mathrm{L}} & -s_{p,\mathrm{L}}(L_4+0.56p) - (L_2+0.34p)\sin(5.83p+0.46) - (L_3+0.47p)\sin(11.18p+3.54) \\ 0 & 1 & 0 & 0 \\ s_{p,\mathrm{L}} & 0 & c_{p,\mathrm{L}} & L_1 + c_{p,\mathrm{L}}(L_4+0.56p) + 0.26p + (L_2+0.34p)\cos(5.83p+0.46) + (L_3+0.47p)\cos(11.18p+3.54) \\ 0 & 0 & 0 & 1 \end{bmatrix}, \tag{7}$$

where

$$\begin{aligned} s_{p,\mathrm{I}} &= \sin(24.5p+14.84), \quad & c_{p,\mathrm{I}} &= \cos(24.5p+14.84), \\ s_{p,\mathrm{L}} &= \sin(18.46p+6.62), \quad & c_{p,\mathrm{L}} &= \cos(18.46p+6.62). \end{aligned} \tag{8}$$

Next, by utilizing only the translation vectors in the last columns of the transformation matrices (6) and (7), we construct the trajectories for the I and L fingertips and joints 1 through 3, as shown in Figure 8. Nonlinearities in the position—pressure mappings can be seen clearly, as well as visual similarities with experimentally obtained positions (Figure 6) and human finger trajectories (Figure 2a), on which we based this research.

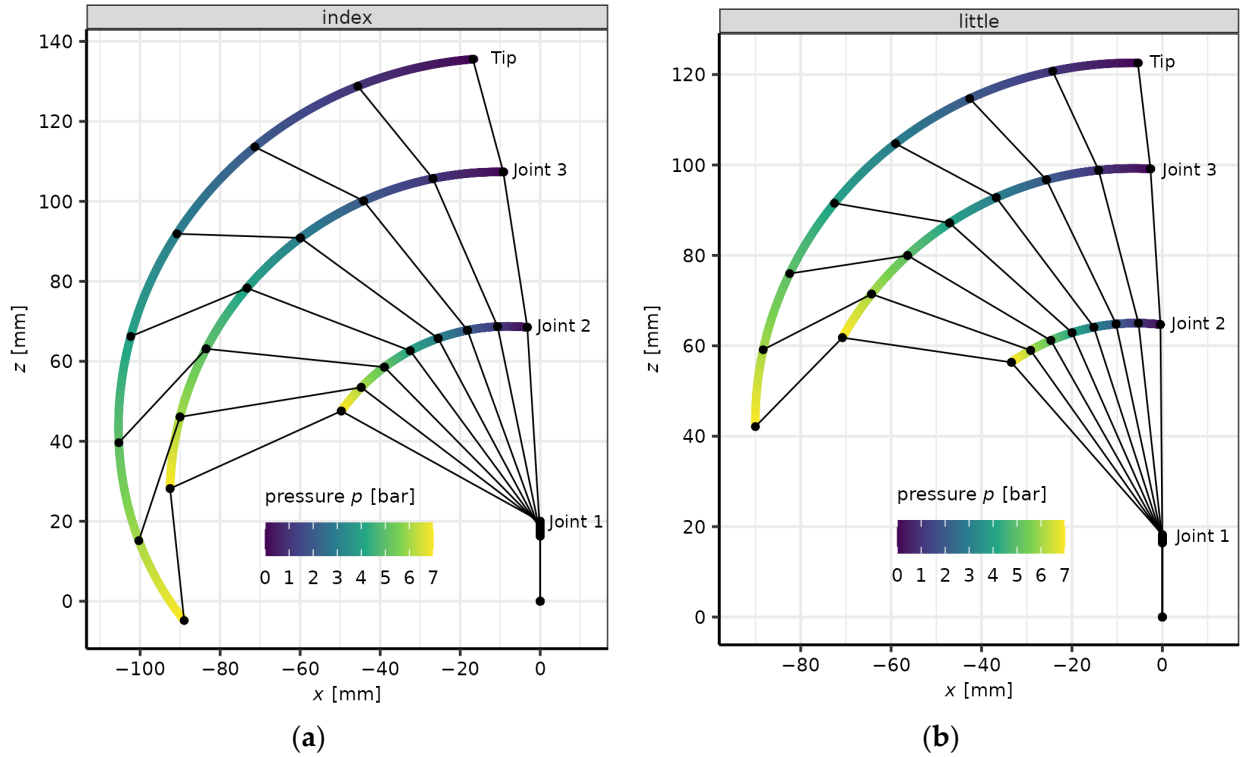


Figure 8. The workspace in the FE plane for: (**a**) I-finger soft actuator and (**b**) L-finger soft actuator. Eight different kinematic positions corresponding to the experimental pressures have been additionally indicated.

Finally, laboratory tests were conducted to evaluate the functionality of the rehabilitation glove prototype. A healthy adult participant voluntarily participated in the experiment and wore the glove (see Figure 5). After fitting, the participant used muscle strength to move their fingers, assessing the glove's ability to support natural movement. Next, a simple experiment simulating the real use of the rehabilitation glove was performed. This involved simultaneously increasing the pressure from 0 to 7 bar in each actuator. At the same time, the participant's hand remained fully relaxed with no muscle engagement (see Figure 5a for the reference position and Figure 5b for the actuated position). This established that the glove continued to function properly, with no delamination of the material. The participant also confirmed the design's ergonomics, noting its ease of use and reporting no pain or fatigue in their fingers or hand after 10 min of wear. Additional simple analyses of the glove's response showed that it can reach the maximum bending angle from the initial to the final position in under one second, which is promising for rehabilitation purposes.

4. Conclusions

In this study, we present a comprehensive approach to the design and development of a rehabilitation glove using a soft robotics approach. The fully 3D-printed glove, powered by compressed air, has the potential for therapeutic support, helping patients restore hand functionality through targeted exercises. It could be employed in various rehabilitation settings, enhancing recovery and promoting independence in daily activities.

We first explore the human finger's workspace based on our previously conducted kinematic analysis of finger movements. We then analyze various existing designs for finger-joint bending actuators and select a hybrid design that combines cylindrical and ribbed geometries with an additional ticker layer as a reinforcing structure. Next, we model and design an innovative asymmetric cylindrical bellow actuator driven by positive pressure. The cylindrical geometry was chosen for its ability to generate maximum blocking force, while the ribbed structure was selected to achieve large bending angles. The design was evaluated using numerical simulations in open-source SOFA software. Our modeling approach varied the actuator's wall thickness to optimize soft robot compliance while maintaining mechanical homogeneity. The simulation results indicate actuators' compatibility and successful replicating of natural human finger movements.

The actuator prototype was 3D-printed using thermoplastic polyurethane (TPU), resulting in a functional rehabilitation glove prototype. Based on the experimental test results, the optimal wall thickness for the soft actuator segments was 0.8 mm. Each finger actuator was tested individually before experiments were conducted on the complete assembly. Testing the finger actuators allowed the evaluation and modeling of angular bending and joint elongations at various pressure levels. The results indicated a strong positive linear correlation between joint angles and input pressure, with small residual errors and coefficients of determination exceeding 98%. A similar linear trend was observed for joint elongation in response to pressure changes, with a minimum R^2 of approximately 95%, demonstrating that the proposed model accurately captures the relationship between joint constraints and movements. These tests allowed us to determine the workspace of the finger actuators and develop a kinematic model applicable to the index (I), middle (M), ring (R), and little (L) finger actuators. We validated this approach using the I and L fingers, with results confirming that the trajectories of the soft actuators closely resemble those of a human index finger. For the final validation, the glove was fitted onto a participant's hand for a voluntary 10 min experiment. The participant confirmed its ergonomic design, emphasizing the advantages of the soft robotics approach.

While the initial results of this study are promising, there is considerable potential for further refinement and optimization of the rehabilitation glove. Implementing separate pneumatic control valves could enable individual finger control, while incorporating proportional pressure control valves could enhance the management of the actuators' bending angles. Additionally, utilizing more flexible materials in 3D printing could improve

bending capabilities and overall comfort. A limitation of this study is the exclusion of the thumb due to its significantly different kinematics. Although 3D-printed, detailed kinematic and workspace analyses were not performed, they will be addressed in future work. This research advances soft robotics in medical rehabilitation, paving the way for enhanced therapeutic devices and improving patient quality of life through the integration of innovative technologies and materials.

Author Contributions: Conceptualization, M.K. and G.G.; methodology, M.K., G.G. and E.K.; software, T.B. and M.K.; validation, G.G.; formal analysis, T.B., G.G. and E.K.; investigation, M.K.; resources, E.K. and G.G.; data curation, T.B.; writing—original draft preparation, G.G., E.K. and T.B.; writing—review and editing, E.K., G.G. and T.B.; visualization, T.B., G.G. and M.K.; supervision, E.K. and G.G.; funding acquisition, E.K. and G.G. All authors have read and agreed to the published version of the manuscript.

Funding: The research was funded by the University of Rijeka Grants uniri-iskusni-tehnic-23-47 and uniri-iskusni-tehnic-23-174.

Data Availability Statement: The data presented in this study are available on request from the corresponding author.

Conflicts of Interest: The authors declare no conflicts of interest.

References

1. Bazina, T.; Mauša, G.; Zelenika, S.; Kamenar, E. Reducing Hand Kinematics by Introducing Grasp-Oriented Intra-Finger Dependencies. *Robotics* **2024**, *13*, 82. [CrossRef]
2. O'Sullivan, S.B.; Schmitz, T.J.; Fulk, G. *Physical Rehabilitation*; FA Davis: Philadelphia, PA, USA, 2019.
3. Chu, C.Y.; Patterson, R.M. Soft robotic devices for hand rehabilitation and assistance: A narrative review. *J. Neuroeng. Rehabil.* **2018**, *15*, 9. [CrossRef] [PubMed]
4. Peng, Z.; Huang, J. Soft rehabilitation and nursing-care robots: A review and future outlook. *Appl. Sci.* **2019**, *9*, 3102. [CrossRef]
5. Lang, C.E.; Lohse, K.R.; Birkenmeier, R.L. Dose and timing in neurorehabilitation: Prescribing motor therapy after stroke. *Curr. Opin. Neurol.* **2015**, *28*, 549–555. [CrossRef] [PubMed]
6. Colombo, R.; Sanguineti, V. (Eds.) *Rehabilitation Robotics: Technology and Application*; Academic Press: Cambridge, MA, USA, 2018.
7. Haggerty, D.A.; Banks, M.J.; Kamenar, E.; Cao, A.B.; Curtis, P.C.; Mezić, I.; Hawkes, E.W. Control of soft robots with inertial dynamics. *Sci. Robot.* **2023**, *8*, eadd6864. [CrossRef] [PubMed]
8. Rus, D.; Tolley, M.T. Design, fabrication and control of soft robots. *Nature* **2015**, *521*, 467–475. [CrossRef] [PubMed]
9. Majidi, C. Soft robotics: A perspective—Current trends and prospects for the future. *Soft Robot.* **2014**, *1*, 5–11. [CrossRef]
10. Cappello, L.; Meyer, J.T.; Galloway, K.C.; Peisner, J.D.; Granberry, R.; Wagner, D.A.; Engelhardt, S.; Paganoni, S.; Walsh, C.J. Assisting hand function after spinal cord injury with a fabric-based soft robotic glove. *J. Neuroeng. Rehabil.* **2018**, *15*, 59. [CrossRef] [PubMed]
11. Polygerinos, P.; Wang, Z.; Galloway, K.C.; Wood, R.J.; Walsh, C.J. Soft robotic glove for combined assistance and at-home rehabilitation. *Robot. Auton. Syst.* **2015**, *73*, 135–143. [CrossRef]
12. Ang, B.W.; Yeow, C.H. Print-it-Yourself (PIY) glove: A fully 3D printed soft robotic hand rehabilitative and assistive exoskeleton for stroke patients. In Proceedings of the 2017 IEEE/RSJ International Conference on Intelligent Robots and Systems (IROS), Vancouver, BC, Canada, 24–28 September 2017; IEEE: Piscataway, NJ, USA, 2017; pp. 1219–1223.
13. Mohammadi, A.; Lavranos, J.; Choong, P.; Oetomo, D. Flexo-glove: A 3D printed soft exoskeleton robotic glove for impaired hand rehabilitation and assistance. In Proceedings of the 2018 40th Annual International Conference of the IEEE Engineering in Medicine and Biology Society (EMBC), Honolulu, HI, USA, 18–21 July 2018; IEEE: Piscataway, NJ, USA, 2018; pp. 2120–2123.
14. Heung, H.L.; Tang, Z.Q.; Shi, X.Q.; Tong, K.Y.; Li, Z. Soft rehabilitation actuator with integrated post-stroke finger spasticity evaluation. *Front. Bioeng. Biotechnol.* **2020**, *8*, 111. [CrossRef] [PubMed]
15. Yi, J.; Chen, X.; Wang, Z. A three-dimensional-printed soft robotic glove with enhanced ergonomics and force capability. *IEEE Robot. Autom. Lett.* **2017**, *3*, 242–248. [CrossRef]
16. Bazina, T.; Kamenar, E.; Zelenika, S.; Črnjarić-Žic, N.; Schnurrer-Luke-Vrbanić, T. Hand model with dependency constrained joints for applications in rehabilitation robotics. *Medicina* **2022**, *58*, 385–398. [CrossRef]
17. Armanini, C.; Boyer, F.; Mathew, A.T.; Duriez, C.; Renda, F. Soft robots modeling: A structured overview. *IEEE Trans. Robot.* **2023**, *39*, 1728–1748. [CrossRef]
18. Craig, J.J. *Introduction to Robotics: Mechanics and Control*, 3rd ed.; Pearson Education: Harlow, UK, 2004.
19. Marchese, A.D.; Katzschmann, R.K.; Rus, D. A Recipe for Soft Fluidic Elastomer Robots. *Soft Robot.* **2015**, *2*, 7–25. [CrossRef] [PubMed]
20. Gregov, G.; Ploh, T.; Kamenar, E. Design, Development and Experimental Assessment of a Cost-Effective Bellow Pneumatic Actuator. *Actuators* **2022**, *11*, 170. [CrossRef]
21. Coevoet, E.; Morales-Bieze, T.; Largilliere, F.; Zhang, Z.; Thieffry, M.; Sanz-Lopez, M.; Carrez, B.; Marchal, D.; Goury, O.; Dequidt, J.; et al. Software toolkit for modeling, simulation, and control of soft robots. *Adv. Robot.* **2017**, *31*, 1208–1224. [CrossRef]

22. Bardin, A.; Le Gac, P.; Cérantola, S.; Simon, G.; Bindi, H.; Fayolle, B. Hydrolytic kinetic model predicting embrittlement in thermoplastic elastomers. *Polym. Degrad. Stab.* **2020**, *171*, 109002. [CrossRef]
23. Mukaka, M.M. A guide to appropriate use of correlation coefficient in medical research. *Malawi Med. J.* **2012**, *24*, 69–71. [PubMed]

Disclaimer/Publisher's Note: The statements, opinions and data contained in all publications are solely those of the individual author(s) and contributor(s) and not of MDPI and/or the editor(s). MDPI and/or the editor(s) disclaim responsibility for any injury to people or property resulting from any ideas, methods, instructions or products referred to in the content.